Catalysis Science & Technology

ROYAL SOCIETY OF CHEMISTRY

PAPER

View Article Online
View Journal | View Issue

Cite this: *Catal. Sci. Technol.*, 2020, **10**, 4264

CO_2 electroreduction on bimetallic Pd–In nanoparticles†

Davide Pavesi, *[ab] Farhan S. M. Ali,[c] Dimitra Anastasiadou,[d] Tanja Kallio, [c] Marta Figueiredo, [d] Gert-Jan M. Gruter,[ae] Marc T. M. Koper[b] and Klaas Jan P. Schouten*[ae]

Received 24th April 2020,
Accepted 16th June 2020

DOI: 10.1039/d0cy00831a

rsc.li/catalysis

CO_2 electroreduction powered by renewable energy is an attractive strategy to recycle air-based carbon. One of the current challenges for the scale up of the technology is that the catalysts that show high faradaic yield at high current density (post-transitional metals such as In, Sn, Bi, Pb) suffer from very high overpotentials of more than 1 V. On the other hand, Pd can convert CO_2 to formate with almost no overpotential, but is readily poisoned by CO and deactivates when trying to reach industrially relevant currents. In this work we show the effect of the interaction of In and Pd in bimetallic nanoparticles, reaching the conclusion that this interaction causes a loss of selectivity towards formate and at the same time suppresses CO poisoning of Pd sites. The results of the catalyst characterization suggest the formation of intermetallic PdIn compounds that in turn cause the aforementioned behavior. Based on these results, it seems that geometric and electronic effects in Pd based intermetallic compounds can alleviate CO poisoning on Pd sites. In the case of PdIn intermetallics this leads to the loss of CO_2 reduction activity, but this strategy may be useful for other electrochemical reactions that suffer from the same problem of deactivation. It remains to be seen if intermetallic compounds of Pd with other elements can yield viable CO_2 reduction catalysts.

Introduction

The electrochemical reduction of CO_2 is an important topic of research nowadays due to the possibility of using renewable electricity to convert this greenhouse gas to value added chemicals and fuels.[1] The reaction can yield several products such as CO, methane, ethylene and formic acid. Among these, formic acid is of particular interest because of its possible use as a liquid fuel precursor and hydrogen carrier for fuel cell applications[2] and because of the existing market as a preservative in animal feed and in the production of leather. The formic acid salt (formate) can be used as precursor to C2 chemicals, thus enabling further conversions.[3,4] The small number of electrons (*i.e.* two) needed for the conversion of CO_2 to formic acid and formate, together with the high atom efficiency, make this conversion one of the economically most promising electrocatalytic conversions. Typically, p-block metals such as Sn, In, Pb, Hg and Bi are used, as they show high selectivity to convert CO_2 into formate. The drawback of using these electrode materials is the very high overpotential needed for the reaction to happen. This is due to the unfavorable potential determining step: the outer sphere electron transfer to form the reactive CO_2^- radical anion. As a result, the reaction requires an overpotential of about 1.2 V, complicating the scale up of the technology due to energy losses.[5]

On the other hand Pd is known to produce formate at very low overpotential *via* an electrohydrogenation mechanism, in which formic acid is generated by the insertion of CO_2 into the Pd–H bond of electrochemically generated surface Pd hydrides. However, the surface of the catalyst is quickly poisoned by concomitant CO formation. This prohibits long-term selectivity to CO_2 reduction products, therefore impeding its practical application in industrial processes.[6,7] In this work, we synthesize bimetallic catalysts based on In (a p-block metal) and Pd to investigate the effect of the coexistence of such different mechanisms on the selectivity and overpotential of CO_2 reduction to formate.

[a] *Avantium Chemicals BV, 1014 BV Amsterdam, The Netherlands. E-mail: davide.pavesi@avantium.com, KlaasJan.Schouten@avantium.com*
[b] *Leiden Institute of Chemistry, Leiden University, PO Box 9502, 2300 RA, Leiden, The Netherlands*
[c] *Electrochemical Energy Conversion Group, Department of Chemistry and Material Science, Aalto University, P.O. Box 16100, 00076 Aalto, Finland*
[d] *Inorganic Materials and Catalysis, Eindhoven University of Technology, P.O. Box 513, 5600 MB Eindhoven, The Netherlands*
[e] *Van 't Hoff Institute for Molecular Sciences, University of Amsterdam, PO Box 94157, 1090 GD Amsterdam, The Netherlands*

† Electronic supplementary information (ESI) available. See DOI: 10.1039/d0cy00831a

Experimental

Materials and chemicals

$InCl_3$ 99.999%, trisodium citrate dihydrate >99%, K_2PdCl_4 99.99%, $NaBH_4$ 99.99% and Nafion© solution (5 wt% solution in lower aliphatic alcohols and water (15–20% water content) were purchased from Aldrich. Vulcan carbon (VXC72R) was purchased from Cabot Corp. Carbon cloth (60% Teflon treated) was obtained from Fuel Cell Store. $KHCO_3$ 99.5% and H_2SO_4 95% solution in water were purchased from Acros Organics.

Particle production and ink formulation

The particles supported on carbon were prepared in water *via* a chemical reduction method. The total amount of moles of metals was kept constant at 0.15 mmol and the ratios of In and Pd were varied in order to achieve different compositions. For the synthesis, an appropriate amount of solid $InCl_3$ was dissolved in about 1.5 mL of ultrapure water (Millipore 18.2 MΩ) along with 353 mg of trisodium citrate dihydrate, and a certain volume of a stock solution of 0.1 M K_2PdCl_4. An overview of the different amounts of salts, as well as the different bimetallic compositions used in this study can be found in Table 1. The resulting solution was diluted in 30 mL of ultrapure water to which 30 mg of carbon black were added under vigorous magnetic stirring. When the carbon was well dispersed in the liquid, the mixture was sonicated for 30 minutes and then placed back on the stirring plate. 7.5 mL of a 0.1 M solution of $NaBH_4$ were added dropwise over the course of 5 minutes and the solution was left to react overnight. The calculated mass loading of metal on carbon was between 36.5% (In only) and 34.8% (Pd only). This number was obtained assuming full reduction of the metal salts on the carbon support.

To clean the particles the mixtures were centrifuged at 11 000 rpm for 10 minutes, discarding the supernatant and refilling the centrifuge tubes with ultrapure water for 3 times and then let dry. The catalyst ink was prepared by resuspending the carbon supported particles in ethanol and adding 250 μL of a Nafion© solution (20% wt ionomer loading in the catalyst) under vigorous stirring. To ensure proper distribution of the ionomer, the inks were sonicated for 30 minutes and then kept stirring for at least 30 more minutes prior to their application to the support. The obtained ink was airbrushed on both sides of a 12 cm^2 carbon cloth and let dry overnight. After this, the electrode was cut in 6 smaller electrodes of 2 cm^2 that were then used for the cyclic voltammetries and bulk electrolysis. The estimated metal loading on the carbon cloth was calculated weighing the electrodes before and after the spraying and assuming that the ratio of catalyst to ionomer remained the same during the airbrushing process.

Table 1 Ratios of salts used for catalyst synthesis. The catalysts are named after the atomic percent of the elements in the final product.

	Composition	
Catalyst	mg $InCl_3$	μL 0.1 M K_2PdCl_4
In/C	33.17	0
In95Pd5/C	31.52	75
In75Pd25/C	24.88	375
In50Pd50/C	16.59	750
Pd/C	0	1500

Electrochemical measurements

Cyclic voltammetry was carried out in a cell connected to a Bio-logic MPG2 (with EC-lab software version 11.10) potentiostat. A leak free Ag/AgCl electrode was used as the reference electrode and the counter electrode was a Pt gauze. The working electrode was carbon cloth with the airbrushed catalytic ink. The electrolyte was a 0.5 M $KHCO_3$ solution, saturated with either CO_2 or N_2 before running the experiments. The electrodes, with an exposed area of 1.5 cm^2 were cycled between −1.5 and 1.3 V *vs.* RHE at a scan rate of 50 mV s^{-1} with N_2 or CO_2 continuously purging the headspace of the cell.

H-cell electrolysis

The controlled potential electrolysis was carried out in an H-cell connected to a Bio-logic MPG2 (with EC-lab software version 11.10) potentiostat. The catholyte was 0.5 M $KHCO_3$ and the anolyte was 0.5 M H_2SO_4. The two chambers were separated by a reinforced Nafion© N324 membrane. The catholyte was continuously purged with CO_2 and stirred to ensure reactant availability on the electrode surface. The potential was applied on the same type of electrodes used for cyclic voltammetry (exposed area of 1.5 cm^2) against a leak free Ag/AgCl electrode and progressively stepped down from −0.5 to −1 to −1.5 V *vs.* RHE in 30 minutes steps. At the end of every step a sample of the catholyte was collected and analyzed for soluble products with a Metrohm 930 compact IC Flex ion chromatographer equipped with a Metrohm Metrosep A supp 7 4 × 250 mm column and a conductivity detector. Gas chromatography was performed on a Varian 4900 micro GC equipped with four modules: CO_x module, MS5 (mol. sieve) module, PPQ (poraplotQ) module and 52C WAX module. The experiments were carried out in the same conditions as above, but the H-cell was sealed and connected to the GC. The head space of the cell was automatically sampled every 4 minutes to detect gaseous products. All the potentials throughout the rest of the manuscript will be referenced to the reversible hydrogen electrode, unless otherwise specified.

Particle characterization

X-ray diffraction patterns of the particles supported on carbon were obtained by a Philips X'pert equipped with X'lerator in a 2θ range from 20 to 80 degrees.

SEM was performed on an Apreo SEM equipped with an energy dispersive X ray (EDX) analyzer. The analysis was performed on the airbrushed electrodes to check the

distribution of Pd and In on the carbon cloths and determine if the theoretical atomic ratios of Pd and In were obtained in the final product. The atomic ratios of Pd and In were measured in different parts of the carbon cloths and averaged to obtain the final result.

Scanning transmission electron microscopy-energy dispersive spectroscopy (STEM-EDX) elemental mapping of PdIn/C and nanoparticle imaging were performed in STEM dark and bright field mode on a JEOL JEM-2800 transmission electron microscope.

X-ray photoelectron spectroscopy measurements were performed on the catalyst powders with a Thermo Fisher K-alpha.

Results

Particle characterization

The distribution of Pd and In on the carbon support and their atomic ratios were investigated with SEM–EDX. The results (Fig. S.I. 1 and Table S.I 1†) show a homogeneous distribution of the elements on the carbon support and an atomic composition very close to the ratios expected from the synthesis, therefore the nominal compositions will be used to refer to the different catalysts. Table S.I. 1† also summarizes the metal loadings on the carbon cloths estimated by weighing the cloths before and after catalyst airbrushing.

Transmission electron microscopy images of the catalyst powders show that the nanoparticles are well distributed on the carbon support. Occasional clustering is observed, especially in In and In rich bimetallic particles. STEM-EDX analysis reveals the coexistence of the elements in the bimetallic particles. In SEM–EDX the compositional information comes from an interaction volume of about 1 μm while in the case of STEM-EDX, due to the small probe size (1 nm), the high accelerating voltage (200 kV) and the thinness of the sample (about 200 nm) the spatial resolution can be as low as 2 nm. STEM-EDX is therefore a viable option to qualitatively assess the coexistence of elements in single nanoparticles. Sample pictures of the nanoparticles on the support, the STEM-EDX analysis and a list of the average particle sizes are summarized in Fig. 1a) and b). More TEM pictures and EDX spectra of the catalysts are available in Fig. S.I. 2 and S.I. 3.†

Generally, the nanoparticles show a rather narrow size range of about 2 to 5 nm, with the particles of pure Pd and In being on average slightly bigger than the bimetallic ones.

Fig. 1c) also shows the XRD patterns of the 5 catalysts. Only the pure Pd nanoparticles give a clear (nano) crystalline response. Pure In and the In–Pd bimetallic catalysts give a flat response that could be ascribed to the small size of the nanocrystals. Determining the crystal structure of very small nanoparticles can be challenging due to the low signal and large background from the catalyst support, requiring a high signal to noise ratio that might not be achievable with laboratory XRD instruments. The solubility of Pd in In is extremely low (as little as a 0.1% addition results in a two phase alloy) and the two elements can form several stable intermetallic compounds with defined stoichiometry and structure such as PdIn (Pd50In50) and $PdIn_3$ (Pd25In75).[8] In their optimal composition ranges, these intermetallics solidify as homogenous phases. Either way, the absence of an XRD response makes it harder to assess the formation of specific alloys or intermetallic compounds.

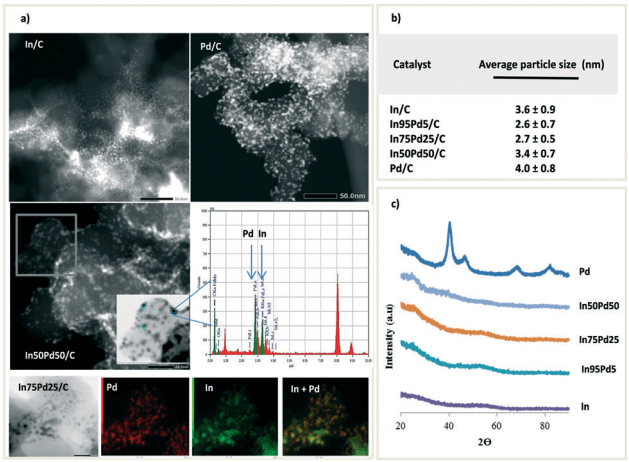

Fig. 1 a) STEM images and STEM-EDX analysis and mapping of some of the catalysts (scale bar of In/C and Pd/C = 50 nm; scale bar of In50Pd50/C and In75Pd25/C = 20 nm). b) The table reports the average particle sizes measured from the TEM images. c) XRD patterns of the 5 catalysts.

Fig. 2 illustrates the binding energy of the Pd^0 3d 5/2 states in pure Pd and in the different In–Pd bimetallic nanoparticles. Increasing amounts of In cause a shift of the binding energy to higher values. The binding energy of Pd is in accordance with tabulated values (335.4 eV), the In50Pd50 shows only a small shift (335.6 eV). The shift becomes more significant in In75Pd25 (336.1 eV). In the case of In95Pd5 the peak deconvolution resulted difficult due to the low Pd signal caused by the small amount of Pd in the sample, therefore the spectrum is not included in the figure. This shift in the

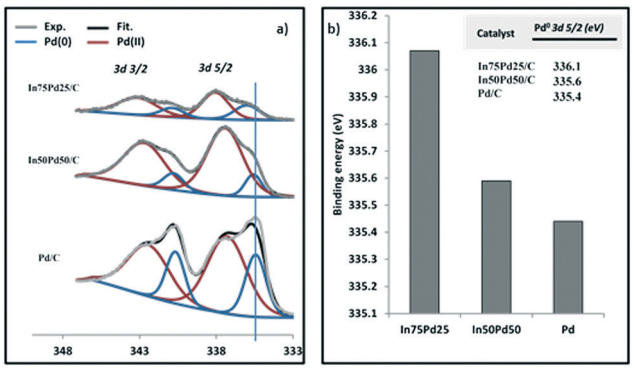

Fig. 2 a) XPS of Pd in Pd and Pd–In bimetallic particles, the line goes through the reference peak of Pd^0 3d 5/2. Notice the shift of the same peak in the bimetallic nanoparticles. b) Tabulated values of the binding energy (B.E.) of the Pd^0 3d 5/2 *vs.* bimetallic particle composition.

binding energy has been reported before to be caused by the formation of intermetallic compounds between Pd and In,[9–12] Pd and Ga[13] and Pd and Zn[14] and is due to several factors affecting the binding energy of core electrons of metals in alloys besides simple charge transfer, such as, in this case, the significant alteration of the valence band of Pd Fig. 1a) caused by the covalent character of the bonds in the intermetallic compounds and the geometrical isolation of the atoms.[13,15,16]

Electrochemical measurements

The electrodes were cycled at a scan rate of 50 mV s^{-1} in N_2 saturated and CO_2 saturated 0.5 M $KHCO_3$ between −1.5 V and 1.3 V *vs.* RHE. The results of the voltammetric analysis are summarized in Fig. 3.

On pure In nanoparticles the current density observed in N_2 is significantly lower than in a CO_2 saturated electrolyte (−23 mA cm^{-2} in N_2 *vs.* −49 mA cm^{-2} in CO_2 at −1.5 V). This is expected, as In is a poor HER electrocatalyst and in the presence of CO_2 higher currents deriving from the concomitant formate production are observed. The redox peaks at approximately −0.2 V and −0.6 V in the voltammetry correspond to the oxidation and reduction of In.

On pure Pd the situation is reversed: the current density in N_2 is significantly higher than in the presence of CO_2 (−100 mA cm^{-2} in N_2 *vs.* −60 mA cm^{-2} in CO_2). Again, this is an expected behavior as Pd is a good HER catalyst and is also known to be poisoned by CO. In the presence of CO_2 a reduction peak attributed to CO adsorption on the surface appears between approximately −0.1 and −0.7 V.[17] At potentials higher than 0.5 V, the adsorbed CO is oxidized, as can be observed in Fig. 3e). Because of the CO accumulation, the surface of the particles is blocked and a lower current output is expected.

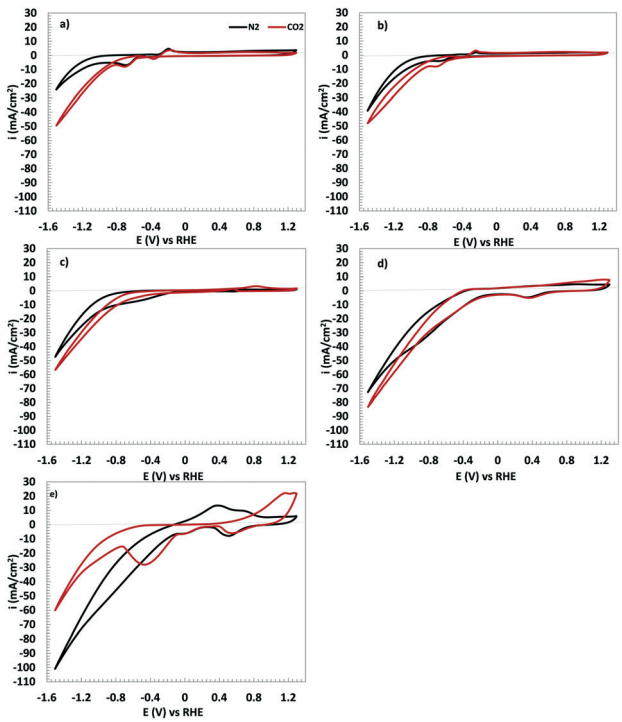

Fig. 3 Cyclic voltammetries in N_2 saturated (black) and CO_2 saturated (red) 0.5 M $KHCO_3$ of a) In/C b) In95Pd5/C c) In75Pd25/C d) In50Pd50/C and e) Pd/C.

On the three alloyed catalysts In95Pd5/C, In75Pd25/C and In50Pd50/C the current densities in CO_2 are higher than in N_2, but the difference is significantly lower than for the pure metals. The presence of CO_2 does not lead to significantly higher currents like in the case of In/C or to significantly lower currents, like in the case of Pd/C. The surface of the catalysts does not seem to be affected by CO poisoning. This is corroborated by the absence of the broad CO adsorption peak between −0.1 and −0.7 V on the bimetallic catalysts (that was instead observed on pure Pd). In the case of In50Pd50/C.

(Fig. 3d)) the CO adsorption peak is not prominent, but it is still possible to observe some CO oxidation above 0.5 V, suggesting that some CO is adsorbing to the surface, but not at the levels observed on pure Pd.

Under N_2 the catalysts become progressively more active for HER with increasing percentage of Pd. This is shown in Fig. S.I. 4,† where it is clearly seen that increasing amounts of Pd shift the onset potential positively and result in higher HER currents. In CO_2 saturated $KHCO_3$, instead, the current density observed on In50Pd50/C is significantly higher than the one observed on pure Pd (−83 mA cm^{-2} *vs.* −60 mA cm^{-2}). These observations tell us that In50Pd50 is a good HER catalyst (although not as good as Pd), and that it is also not prone to CO poisoning. The overlap of the cyclic voltammetries of the catalysts in CO_2 saturated $KHCO_3$ is in Fig. S.I. 5.†

Additional information can be gathered by the shape of the cyclic voltammetries. The In75Pd25/C and In50Pd50/C catalysts don't show redox peaks associated with In or Pd. In fact, the CVs are very different than the ones of the parent elements and do not seem to be a simple combination of the two, indicating that a new intermetallic phase may be formed. In the case of In95Pd5/C the CV closely resembles the one of In (the redox peaks of unalloyed In are visible), albeit reaching higher currents in the reaction region in N_2. No peaks related to Pd are observed in this CV. This could indicate that a large amount of unalloyed In is present, with minor amounts of intermetallic PdIn compounds causing the higher HER activity.

H-cell electrolysis

The 5 catalysts, airbrushed on a carbon cloth electrode support, were tested in an H-cell with CO_2 saturated 0.5 M $KHCO_3$ as catholyte. The electrodes were held at −0.5, −1 and −1.5 V for 30 minutes each. Fig. 4 summarizes the faradaic yields (FY) of the 5 different catalysts at the 3 potentials investigated.

In line with previous literature,[5] pure In produces formate with a high selectivity of about 70% at a potential of −1 V.

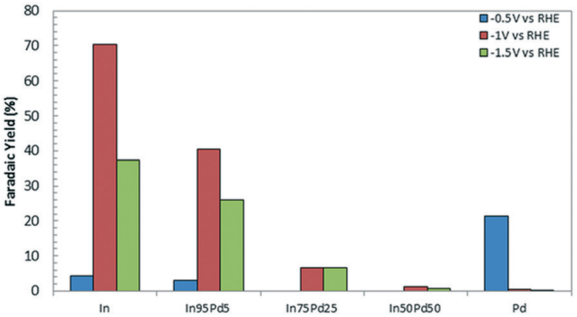

Fig. 4 Faradaic yield towards formate of the 5 catalysts at −0.5 V *vs.* RHE (blue); −1 V *vs.* RHE (red) and −1.5 V *vs.* RHE (green).

Basically no formate is observed at −0.5 V and at −1.5 V there is loss of selectivity likely due to mass transport limitations.

It is known that Pd can produce formate at very low overpotential (a narrow window close to 0 V at neutral pH) before the surface becomes blocked with strongly adsorbed CO at higher applied potentials[6] (potentials that are nonetheless required to reach the high currents needed for practical applications). This is also what we observe, as the Pd catalyst is producing formate with low FY at −0.5 V (already 0.5 V negative of the onset potential) before becoming completely deactivated at higher potentials.

There is a clear trend of loss of selectivity towards formate as the percentage of Pd in the catalyst is increased. At −1 V going from pure In to In95Pd5, In75Pd25 and In50Pd50 the selectivity to formate decreases from 70% on pure indium to respectively 40%, 7% and 1.5%. Starting on the right side of the graph at −0.5 V, the selectivity goes from about 22% on pure Pd to 0.7% in the In50Pd50 catalyst. Clearly, the In50Pd50 catalyst has lost selectivity towards formate at any applied potential.

To confirm that the loss of selectivity towards formate is due to inhibition of CO_2 reduction in general and not, for example, due to the shift of selectivity in the bimetallic catalysts to gaseous CO_2 reduction products, online gas chromatography was performed on the five catalysts during bulk electrolysis. Except for minor amounts of CO being evolved on Pd at −1.5 V, for the other materials it was found that gaseous CO_2 reduction products were below the detection limit of the GC and that the main gaseous product was H_2 (see Fig. S.I. 7†).

Discussion

Pd and In are producing formate with different mechanisms: CO_2 reduction on Pd is believed to proceed through an electrohydrogenation mechanism. CO_2 is converted to formate by electrochemically generated surface Pd hydride at potentials close to the equilibrium potential of CO_2 reduction to formate,[6] this would happen by insertion of CO_2 into the Pd–H bond. On In we have a proton decoupled electron transfer to form the radical anion, subsequently leading to formate.[5] This is the proposed reaction mechanism for formate-forming post transition metals, as it is known that CO_2 interacts very weakly with their surface. The standard potential of this first outer sphere reaction is −1.9 V *vs.* SHE.[18] We show here that the interaction of the two elements is detrimental to formate selectivity in the alloyed catalysts and this can be ascribed to geometrical and electronic effects in the bimetallic particles.

PdIn bimetallic nanoparticles have been studied for heterogeneous catalysis applications before and the formation of intermetallic compounds has been confirmed. According to the synthesis method it is possible to obtain the stoichiometric intermetallic compounds or a preferential phase (usually PdIn), with excess In or Pd remaining unalloyed.[19,20] The formation of these regular intermetallic structures breaks the ensemble of Pd atoms, resulting in significant alterations of the binding modes and strengths of atoms and molecules over them. In particular, CO can only adsorb linearly on the isolated Pd atoms and the interaction strength decreases significantly with increasing amounts of In.[19–21] Moreover, H_2 chemisorption was also found to be hindered on PdIn bimetallic catalysts.[21]

A similar behavior is observed in PdGa intermetallic catalysts.[13] Increasing the Ga : Pd ratio leads to a higher partial negative charge on Pd. The change in electronic structure deriving from this phenomenon and the partially covalent character of the Pd–Ga bonds strongly influences the adsorption properties of these intermetallic compounds. Adsorption of CO on PdGa surfaces is significantly hindered and the molecule can be desorbed completely from the surface at 250 degrees less than on pure Pd.[22]

As was already discussed above, CO_2 reduction to formate on Pd proceeds through an electrohydrogenation mechanism that involves the insertion of CO_2 into Pd–H bonds of surface hydrides generated electrochemically. The first generated HCO_2 intermediate could leave the surface immediately or be bound to it through either one (monodentate) or both (bidentate) its oxygen atoms.[23] The geometrical isolation of the Pd atoms in the intermetallic compound would exclude the formation of the bidentate intermediate, since the neighboring In atoms are very unlikely to take part in the bonding of molecules to the surface. Moreover, the monodentate intermediate could be bound more weakly to Pd sites for the same electronic reasons discussed above, and one could imagine that in fact there is no formate-like adsorbed intermediate. In such a situation, the selectivity of hydrogen or formate formation would depend on the rate of the surface hydride reaction either with water or with CO_2.

Alternatively, the loss of selectivity could be ascribed to a change in the properties of the surface Pd hydride. A change in the electronic structure of the catalytic surface could alter the charge distribution between the Pd and the H, turning a reactive hydride, able to react with CO_2, into something more similar to an adsorbed hydrogen and therefore steering the selectivity towards HER. The suppression of surface Pd hydride formation has been observed before in PdGa intermetallics and has been ascribed to the covalent Pd–Ga

interaction, which is absent in Pd and conventional Pd alloys.[24,25] A similar situation could be arising from the interaction between Pd and In.

It has been argued that the intrinsically strong Pd–H bond is responsible for the high formate selectivity of Pd at low overpotential.[26] However, hydrogen adsorption energy is correlated with CO adsorption energy, making it difficult to separate formate production from CO poisoning.[27] Pd electrocatalysts tested in potential ranges similar to the ones in this study (*i.e.* more negative than the potentials at which formate production is favored) have been reported to either produce significant amounts of CO, although with different selectivities[28,29] or to be mainly poisoned by this product, evolving only small amounts of CO in the gas phase.[6,30] These incongruences can be ascribed to differences in the electrocatalyic environment or to the nature of the active sites on Pd catalysts synthesized with different methods.[31] At the three potentials investigated, our Pd catalyst seems to be mostly poisoned by CO, as also observed in the cyclic voltammetry.

A previous report[30] found a PdIn catalyst to be selective towards CO evolution. Since Pd and In are known to form several compounds, it is possible that Pd-rich PdIn intermetallics can evolve CO selectively by lowering the binding energy of CO to the surface, while In-rich intermetallics will avoid the CO pathway altogether by lowering the binding energy of intermediates involved in the CO evolution pathway. The absence (or significant reduction) of CO adsorption observed in the CVs of the bimetallic catalysts in this study means that the adsorption energy of CO (or CO intermediates) on Pd sites is significantly lower than in pure Pd, and since the adsorption energy of hydrogen is related, it would mean that it is similarly weakened, leading to the loss of both CO poisoning and formate selectivity. Theoretical calculations would be needed to better understand the underlying mechanism.

The above reasoning explains the observed behavior of the bimetallic catalysts. At −0.5 V pure Pd is able to generate formate with appreciable selectivity, while Pd sites in bimetallic particles are not able to do so. This is because of the hindering of the interaction of the CO_2 with the surface or the absence of the reactive surface Pd hydride. Moreover, since the surface doesn't become poisoned by CO, Pd sites retain their HER activity, although somehow lowered by the interaction with neighboring In (see Fig. S.I. 4†). This means that at higher applied potentials the current is mostly sustained by these active HER sites, avoiding the higher overpotential pathway of CO_2 reduction on the In sites (which may as well be changed by the interaction with the Pd). This is in fact observed, as pure In particles show a good selectivity towards formate at −1 and −1.5 V, while the more Pd rich bimetallic catalysts (In75Pd25/C and In50Pd50/C) fail to reduce CO_2 at these potentials as well. An exception is In95Pd5/C. Fig. S.I. 6b†) illustrates the concentrations of formate at the end of every potential step during bulk electrolysis. In/C and In95Pd5/C reach the same concentration of formate at the end of every step. This means that the productivity of formate from unalloyed indium sites is the same, but the separate HER contribution to the current of Pd sites in the intermetallic phase lowers the faradaic yield (In95Pd5 reaches higher current densities at every potential, as shown in Fig. S.I. 6a†). Probably a sum of CO_2 reduction on unalloyed In and HER on PdIn sites). As discussed above, this is confirmed by the cyclic voltammetries: In95Pd5 is the only bimetallic catalyst that still shows the characteristic redox features of unalloyed In (but no features of Pd), while in In75Pd25 and In50Pd50 the CVs change drastically (see Fig. 3), probably due to the predominant presence of PdIn intermetallic phases. Fig. S.I. 6† also shows that on the other alloyed catalysts the productivity of formate drops drastically, suggesting the absence of unalloyed In sites.

In this study, we were not able to show the preferential formation of specific intermetallic compounds. However, we think that the formation of the intermetallic phases is happening for a few reasons. First, the Pd and In elements are found to share space in the same nanoparticles with STEM-EDX (see Fig. 1). This does not automatically mean that the elements are properly alloyed, but if this was not the case, one would expect to see a sum of the activities of In and Pd in the bimetallic catalysts. This would mean that the CO adsorption and stripping peaks would be visible in the CV of the bimetallic catalysts, and that we would be observing CO_2 reduction to formate at every potential: from Pd sites at −0.5 V and from In sites at −1 V and −1.5 V.

Moreover, the formation of intermetallic compounds is thermodynamically favorable. The formation of a solid solution alloy has typical ΔH_f between 0 and −10 kJ mol^{-1} while, for example, the formation of the intermetallic compound PdIn has a ΔH_f of −61.4 kJ mol^{-1}.[32] Therefore there is an appreciable thermodynamic drive to form intermetallic phases based on Pd and In.

Additional evidence is brought by the shift to higher binding energies of the Pd^0 3d 5/2 orbital in the XPS of the bimetallic particles (see Fig. 2). As discussed above, this is a well-documented indication of intermetallic compound formation between Pd and In.

Conclusions

We have shown that the interaction of In and Pd in In–Pd bimetallic catalysts is detrimental to the selectivity towards formate of these catalysts. When mixed together, In seems to act as an agent that weakens the interaction of CO_2 with the surface, therefore preventing CO poisoning and electrohydrogenation altogether. This causes the Pd sites in PdIn catalysts to evolve hydrogen freely even in CO_2 saturated environments, making all the current go through this reaction and impeding the high overpotential electron transfer on In from happening even at high applied potentials. Although the effects on formate selectivity and activity towards CO_2 reduction are not encouraging, we have observed that it is possible to attenuate and even prevent CO

poisoning on Pd based catalysts. These catalysts would be the preferred ones to catalyze the reduction of CO_2 to formate since they would allow to carry out the reaction at almost 1.2 V lower cell voltage in equal conditions when compared with p-block based catalysts. Therefore, using low amounts of In or other post transitional metals in Pd matrices may be a strategy to hinder or prevent CO poisoning. At the same time, the right combination of geometric and electronic effects may allow the retention of some selectivity towards formate. This result would be promising to pursue an energy efficient, big scale electrochemical CO_2 conversion to formate.

Conflicts of interest

There are no conflicts to declare.

Acknowledgements

This research has been supported by the European Commission (Research Executive Agency) grant Elcorel (Nr 722614) under the Marie Sklodowska-Curie Innovative Trainings Network. This work made use of Aalto University Nano Microscopy Center (Aalto-NMC) facilities.

References

1 Z. W. Seh, J. Kibsgaard, C. F. Dickens, I. Chorkendorff, J. K. Nørskov and T. F. Jaramillo, *Science*, 2017, **355**, 6321.
2 X. Lu, D. Y. C. Leung, H. Wang, M. K. H. Leung and J. Xuan, *ChemElectroChem*, 2014, **1**, 836.
3 M. C. Boswell and J. V. Dickson, *J. Am. Chem. Soc.*, 1918, **40**, 1779.
4 T. Meisel, Z. Halmos, K. Seybold and E. Pungor, *J. Therm. Anal.*, 1975, **7**, 73.
5 Y. Hori, *Mod. Aspects Electrochem.*, 2008, **42**, 89.
6 X. Min and M. W. Kanan, *J. Am. Chem. Soc.*, 2015, **137**, 4701.
7 R. Kortlever, I. Peters, S. Koper and M. T. M. Koper, *ACS Catal.*, 2015, **5**, 3916.
8 J. R. Knight and D. W. Rhys, *J. Less-Common Met.*, 1959, **1**, 292.
9 A. García-Trenco, A. Regoutz, E. R. White, D. J. Payne, M. S. P. Shaffer and C. K. Williams, *Appl. Catal., A*, 2018, **220**, 9.
10 C. Rameshan, H. Lorenz, L. Mayr, S. Penner, D. Zemlyanov, R. Arrigo, M. Haevecker, R. Blume, A. Knop-Gericke, R. Schlögl and B. Klötzer, *J. Catal.*, 2012, **295**, 186.
11 T. Skála, K. Veltruská, M. Moroseac, I. Matolínová, G. Korotchenkov and V. Matolín, *Appl. Surf. Sci.*, 2003, **205**, 196.
12 G. M. McGuirk, J. Ledieu, É. Gaudry, M.-C. de Weerd and V. Fournée, *J. Chem. Phys.*, 2014, **141**, 084702.
13 M. Armbrüster, R. Schlögl and Y. Grin, *Sci. Technol. Adv. Mater.*, 2014, **15**, 034803.
14 P. Kast, M. Friedrich, F. Girgsdies, J. Kröhnert, D. Teschner, T. Lunkenbein, M. Behrens and R. Schlögl, *Catal. Today*, 2016, **260**, 21.
15 M. Weinert and R. E. Watson, *Phys. Rev. B: Condens. Matter Mater. Phys.*, 1995, **51**, 17168.
16 W. Olovsson, C. Göransson, L. V. Pourovskii, B. Johansson and I. A. Abrikosov, *Phys. Rev. B: Condens. Matter Mater. Phys.*, 2005, **72**, 064203.
17 R.-H. Guo, C.-F. Liu, T.-C. Wei and C.-C. Hu, *Electrochem. Commun.*, 2017, **80**, 24.
18 Y. Hori, H. Wakebe, T. Tsukamoto and O. Koga, *Electrochim. Acta*, 1994, **39**(11/12), 1833.
19 Z. Wu, E. C. Wegener, H.-T. Tseng, J. R. Gallagher, J. W. Harris, R. E. Diaz, Y. Ren, F. H. Ribeiro and J. T. Miller, *Catal. Sci. Technol.*, 2016, **6**, 6965.
20 J. L. Snider, V. Streibel, M. A. Hubert, T. S. Choksi, E. Valle, D. C. Upham, J. Schumann, M. S. Duyar, A. Gallo, F. Abild-Pedersen and T. F. Jaramillo, *ACS Catal.*, 2019, **9**, 3399.
21 J. Ye, Q. Ge and C.-J. Liu, *Chem. Eng. Sci.*, 2015, **135**, 193–201.
22 Dirk Rosenthal, Roland Widmer, Ronald Wagner, Peter Gille, Marc Armbrüster, Yuri Grin, Robert Schlögl and Oliver Gröning, *Langmuir*, 2012, **28**, 6848.
23 Ruud Kortlever, Jing Shen, K. J. P. Schouten, F. C. Vallejo and M. T. M. Koper, *J. Phys. Chem. Lett.*, 2015, **6**, 4073.
24 A. Borodzinski and G. C. Bond, *Catal. Rev.: Sci. Eng.*, 2006, **48**, 91.
25 K. Kovnir, D. Teschner, M. Armbrüster, P. Schnörch, M. Hävecker, A. Knop-Gericke, Y. Grin and R. Schlögl, *BESSY Highlights*, 2007, 22.
26 C. W. Lee, N. H. Cho, K. T. Nam, Y. J. Hwang and B. K. Min, *Nat. Commun.*, 2019, **10**, 3919.
27 J. S. Yoo, R. Christensen, T. Vegge, J. K. Nørskov and F. Studt, *ChemSusChem*, 2016, **9**, 358.
28 D. Gao, Z. Hu, F. Cai, D. Wang, Y. Hu, B. Jiang, W.-B. Cai, X. Chen, R. Si, F. Yang, S. Miao, J. Wang, G. Wang and X. Bao, *Nano Res.*, 2017, **10**, 2181–2191.
29 W. Sheng, S. Kattel, S. Yao, B. Yan, Z. Liang, C. J. Hawxhurst, Q. Wuc and J. G. Chen, *Energy Environ. Sci.*, 2017, **10**, 1180–1185.
30 W. Luo, W. Xie, M. Li, J. Zhanga and A. Züttel, *J. Mater. Chem. A*, 2019, **7**, 4505–4515.
31 A. Klinkova, P. De Luna, C.-T. Dinh, O. Voznyy, E. M. Larin, E. Kumacheva and E. H. Sargent, *ACS Catal.*, 2016, **6**, 8115–8120.
32 S. Furukawa and K. Takayuki, *ACS Catal.*, 2017, **7**, 735.

